FORM TI-12
07/1999

B-T-3291

INTERFACIAL STRUCTURES OF CONFINED AIR-WATER TWO-PHASE BUBBLY FLOW

S. Kim and M. Ishii
(Purdue University)

Q. Wu and D. McCreary
(Oregon State University)

S. G. Beus
(Bettis)

DE-AC11-98PN38206

BETTIS ATOMIC POWER LABORATORY WEST MIFFLIN, PENNSYLVANIA 15122-0079

Operated for the U.S. Department of Energy
by Bechtel Bettis, Inc.

DISCLAIMER

INTERFACIAL STRUCTURES OF CONFINED AIR-WATER TWO-PHASE BUBBLY FLOW

S. Kim and M. Ishii
Thermal Hydraulics and Reactor Safety Lab,
School of Nuclear Engineering, Purdue University,
West Lafayette, IN 47907

*Q. Wu and *D. McCreary
Department of Nuclear Engineering,
Oregon State University,
Corvallis, OR 97331

S. G. Beus
Bettis Atomic Power Laboratory,
Bechtel Bettis, Inc.,
Post Office Box 79,
West Mifflin, PA 15122-0079,

**The author was at Purdue University when this work was done.*

ABSTRACT

The interfacial structure of the two-phase flows is of great importance in view of theoretical modeling and practical applications. In the present study, the focus is made on obtaining detailed local two-phase parameters in the air-water bubbly flow in a rectangular vertical duct using the double-sensor conductivity probe. The characteristic wall-peak is observed in the profiles of the interfacial area concentration and the void fraction. The development of the interfacial area concentration along the axial direction of the flow is studied in view of the interfacial area transport

and bubble interactions. The experimental data is compared with the drift flux model with C_0=1.35.

1. INTRODUCTION

In two-phase flows, the interfacial area concentration and void fraction are key geometric parameters in interfacial transport and heat transfer phenomena. While the void fraction serves as an indispensable parameter in view of hydrodynamics and thermodynamics, the interfacial area concentration is directly related to the interfacial transport of mass, momentum, and energy. Therefore, the detailed local information of the two parameters is of supreme importance in order to assess the given two-phase flow systems accurately.

In the formulation of the two-fluid model[1], each of the two phases is considered separately. However, since the two-fluid model employs an averaging method in the formulation, the averaged macroscopic field equations of each phase contain phase interaction terms. Hence, the constitutive relations specifying the interfacial transfer terms are necessary in order to apply the two-fluid model in practice effectively. Therefore, the detailed local database is indispensable in establishing the constitutive relation for the interfacial area concentration.

In view of practical applications, Ishii and Mishima[2] simplified the two-fluid model as

$$\frac{\partial \alpha_k \rho_k}{\partial t} + \nabla \cdot (\alpha_k \rho_k v_k) = \Gamma_k \quad : Continuity \tag{1}$$

$$\frac{\partial \alpha_k \rho_k v_k}{\partial t} + \nabla \cdot (\alpha_k \rho_k v_k v_k) = -\alpha_k \nabla p_k + \nabla \cdot \alpha_k (\bar{\tau} + \tau_k') + \alpha_k \rho_k g + v_{ki} \Gamma_k + M_{ik} - \nabla \alpha_k \cdot \tau_i : Momentum, \tag{2}$$

$$\frac{\partial \alpha_k \rho_k H_k}{\partial t} + \nabla \cdot (\alpha_k \rho_k H_k v_k) = -\nabla \cdot \alpha_k (\bar{\bar{q}}_k + q_k') + \alpha_k \frac{D_k}{Dt} p_k + H_{ki} \Gamma_k + \frac{q''_{ki}}{L_s} + \phi_k : Enthalpy\ Energy, \tag{3}$$

where Γ_k, M_{ik}, τ_i, q''_{ki} and ϕ_k are the mass generation, generalized interfacial drag, interfacial shear stress, interfacial heat flux and dissipation, respectively, with the subscript i denoting the value at the interface. Here, L_s denotes the length scale at the interface, where $1/L_s$ has the physical meaning of the interfacial area per unit mixture volume[1], such that

$$\frac{1}{L_s} = a_i : \qquad \text{interfacial area per unit mixture volume} \tag{4}$$

In equations (1) through (3), the interfacial transfer terms can be modeled such that[1-5]

$$\Gamma_k \equiv a_i m_k : \qquad \text{Generation of Mass,} \tag{5}$$

$$M_{id} = \frac{\alpha_d F_D}{B_d} + \frac{\alpha_d F_V}{B_d} + \frac{9}{2}\frac{\alpha_d}{r_d}\sqrt{\frac{\rho_c \mu_m}{\pi}}\int_t \frac{D_d}{D\xi}(v_d - v_c)\frac{d\xi}{\sqrt{t-\xi}} : \text{Generalized Drag,} \tag{6}$$

$$\Gamma_k H_{ki} + \frac{\dot{q}_{ki}}{L_s} = a_i\left[m_k H_{ki} + h_{ki}(T_i - T_k)\right] : \text{Interfacial Energy Transfer.} \tag{7}$$

Here, m_k, F_D, B_d, F_V, and μ_m are the mean mass transfer rate, standard drag force, volume of a typical dispersed fluid particle, virtual mass force and mixture viscosity, respectively. With the last term in the right hand side of equation (6) being the Basset force, the interfacial transfer term due to standard drag can be written in terms of interfacial area concentration[2,5] such that

$$\frac{\alpha_d F_D}{B_d} = -a_i\left[\frac{C_D}{4}\left(\frac{r_{sm}}{r_D}\right)\frac{\rho_c v_r |v_r|}{2}\right] \tag{8}$$

For the interfacial energy transfer term, the interfacial heat flux, q''_{ki} can be modeled using the driving force or the potential for an energy transfer. Hence, in equation (7), T_i and T_k are the temperature at the interface and the bulk temperature based on the mean enthalpy, and h_{ki} is the interfacial heat transfer coefficient. By examining the equations (5) through (8), the importance of the interfacial area concentration is evident. As can be seen in the equations, the phase interaction terms are expressed in terms of interfacial area concentration and the driving force such that

$$\text{(Interfacial Transfer Term)} \sim a_i \times \text{(Driving Force)} \tag{9}$$

This implies that the closure relation and the detailed measurement method for the interfacial area concentration are indispensable for accurate assessment of the given two-phase flows using the two-fluid model.

In efforts of solving this closure problem in the two-fluid model, Kocamustafaogullari and Ishii[6] generalized the population balance approach suggested by Reyes[7] and established the foundation for developing the interfacial area transport equation. Recently, the one-group interfacial area transport equation for dispersed bubbles was formulated by Wu et al.[8]. Nevertheless, the database for the model to be evaluated for the flows in a rectangular duct is far short from being sufficient. Therefore, it is one of the objectives of the present study to establish a

solid database for the evaluation of the model. Another important aspect of the present study can be found in its geometry of the flow duct. Most of the two-phase flow experiments have been performed in the round tubes, and only a few studies[9-12] can be found for the two-phase flows in the rectangular duct geometry. Furthermore, these studies focused on flow regime identification or two-phase friction factor studies. There have been no experimental studies yet to evaluate the axial development or lateral profiles of the local two-phase parameters. Therefore, the local measurement of the two-phase flow parameters can be invaluable for understanding the interfacial structure in a rectangular flow duct and in practical applications.

2. DEVELOPMENT OF THE LOCAL CONDUCTIVITY PROBE TECHNIQUE

The conductivity probe has been one of the most widely used measurement techniques in obtaining local two-phase flow parameters[13-20]. It was first proposed by Neal and Bankoff[13] accounting for the fundamental differences in conductivity between water and air. In an air-water two-phase mixture, the characteristic rise/fall of impedance signals from the sensor(s) can be acquired as bubbles pass through the sensor(s). With the acquired signals from the sensor, the local time-averaged void fraction can be easily obtained by dividing the sum of the time fraction occupied by gas-phase by the total measurement time. Furthermore, its capability of measuring the local interfacial velocity of bubbles with multiple sensors makes the conductivity probe the most popular measurement technique in recent experimental studies[15-17,19,20,22]..

The measurement principle of the double-sensor conductivity probe in obtaining local time-averaged interfacial area concentration, a_i, is based on the definition given by Ishii[1], where the local time-averaged $\bar{a}_i^t$ is defined by

$$\bar{a}_i^t = \frac{1}{\Delta T}\sum_j \left(\frac{1}{|\boldsymbol{v}_i \cdot \boldsymbol{n}_i|} \right)_j \tag{10}$$

where j denotes the j^{th} interface which passes a local point during the time interval, ΔT. Here, $\boldsymbol{v}_i$ and $\boldsymbol{n}_i$ are the bubble interfacial velocity and unit surface normal vector of the j^{th} interface, respectively. Equation (10) implies that the local interfacial area concentration can be obtained from the bubble interfacial velocity. In view of equation (10), Kataoka et al.[14] formulated a mathematical method to determine the local time-averaged interfacial area concentration for both

double-sensor and four-sensor probes. In the application of the double-sensor probe, it was suggested that

$$\tilde{a}_i^t(x_0,y_0,z_0) = 2N_t \overline{\frac{1}{|v_i|\cos\phi}} \tag{11}$$

with

$$\overline{\frac{1}{|v_i|}} = \sum_j \frac{1}{|v_{ij}|} \Big/ \sum_j \quad \text{and} \quad \overline{\frac{1}{\cos\phi}} = \sum_j \frac{1}{\cos\phi_j} \Big/ \sum_j \ , \tag{12}$$

where N_t is the number of bubbles which pass the point (x_0,y_0,z_0) per unit time, and ϕ_j= angle between the unit normal of the j^{th} interface and the interfacial velocity as shown in Figure 1.

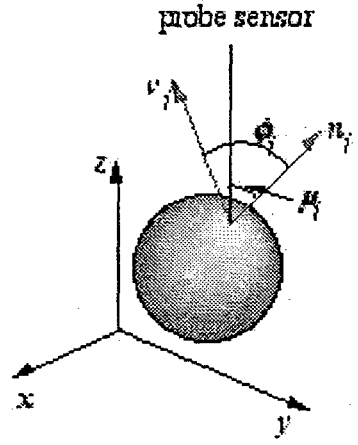

Figure 1. Definition of angles ϕ_j and μ_j.

In formulating equation (11), however, it should be noted that the bubbles are assumed to be spherical, and every part of the bubble is assumed to have equal probability of being intersected by the probe. It was also assumed that the angle between the bubble interfacial velocity and the axial direction z, was random with an equal probability within some maximum angle, α_0. The final expression for the local time-averaged interfacial area concentration by the double-sensor probe technique was then given by[14]

$$\tilde{a}_i^t(x_0,y_0,z_0) = \frac{4N_t\left\{\sum_j \frac{1}{|v_{szj}|}\Big/\sum_j\right\}}{1-\cot\frac{1}{2}\alpha_0 \ln\left(\cos\frac{1}{2}\alpha_0\right)-\tan\frac{1}{2}\alpha_0 \ln\left(\sin\frac{1}{2}\alpha_0\right)} \tag{13}$$

where α_0 was obtained by

$$\frac{\sin 2\alpha_0}{2\alpha_0} = \frac{1-\left(\sigma_z^2/\overline{|v_{iz}|}^2\right)}{1+3\left(\sigma_z^2/\overline{|v_{iz}|}^2\right)} \tag{14}$$

Here, v_{szj}, $\overline{|v_{iz}|}$, and σ_z are the z-component of the j^{th} interfacial velocity, mean value of the z-component of the velocity, and the z-component velocity fluctuations, respectively. Also, v_{szj} was defined by

$$|v_{szj}|\cos\mu_j = |v_{ij}|\cos\phi_j \tag{15}$$

where the angle μ_j was defined as the angle between the probe sensor and the normal surface vector as shown in Figure 1. The reciprocal harmonic mean of $|v_{szj}|$ and the square mean of fluctuationσ_z^2 were further correlated with the probability density function. For detailed derivation, one should refer to the study done by Kataoka et al.[14].

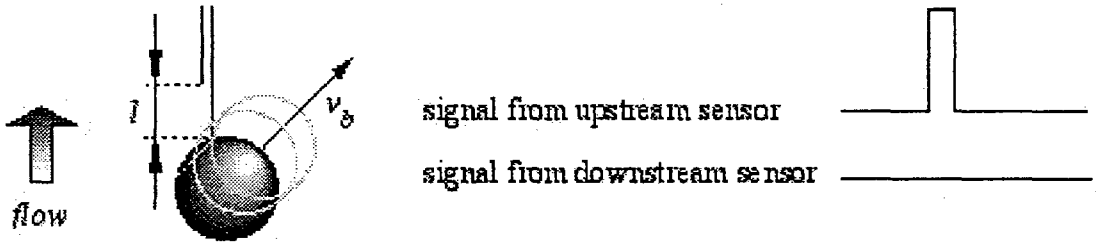

Figure 2. Schematic illustration of the missing bubble phenomenon.

The application of equation (13), however, may result in an erroneous estimation of the interfacial concentration. This is due to the fact that the mathematical formulation given by Kataoka et al.[14] does not account for the fluctuations of the bubble as it penetrates and pass through the sensors of the probe. Moreover, the passing bubbles do not necessarily pass through both sensors of the probe, resulting in 'missing' phenomenon as illustrated in Figure 2. Such shortcomings have been identified in the several studies[16,18,21,22]. In view of this, Wu and Ishii[21] recently suggested a modified equation accounting for the bubble fluctuations and the

missing phenomenon in the application of the double-sensor conductivity probe. In this study, they considered the effects of the lateral movement of the bubbles and the probe tip spacing (l in Figure 2). They categorized the measured bubbles into two, one for bubbles whose interface is passing through both sensors, and another for those missing one of the sensors of the probe. In their correction scheme, the mean value of the experimentally measured bubble interfacial velocity was rigorously related to the actual interfacial velocity of the bubbles by defining theoretical calibration factors. These calibration factors were employed to account for the bubbles whose interfaces move normal to the probe, and those missing one of the sensors. By determining the calibration factors, they modified the formula[21] given by Kataoka et al.[14] as

$$\bar{a}_i^t = f_{total}\left(\frac{2N_b}{\Delta s \Delta T}\right)\left(\frac{\sum_j (\Delta t_j)}{N_b - N_{miss}}\right), \text{ for } \Delta s = 0.36\, D_b \sim 0.86\, D_b \quad (21)$$

with

$$f_{total} = 2 + \left(\frac{\dot{v}_b}{\bar{v}_b}\right)^{2.25}, \text{ for } \Delta s = 0.36\, D_b \sim 0.86\, D_b \quad (22)$$

where

N_b = number of total bubbles obtained,

$\dot{v}_b$ = fluctuation of bubble velocity,

$\bar{v}_b$ = average bubble velocity obtained by effective signals,

Δt_j = time delay obtained by effective signals for the j^{th} bubble interface, and

Δs = distance between two tips of the sensors.

Equation (21) was found to be valid as long as the output signals from the probe were valid for bubble identification and the sample size was sufficiently large. For bubble sizes varying from 0.6 to 1.4 times the mean bubble size, it was found that the interfacial area concentration calculated by equation (21) would result in a statistical error of ± 7% for a sample size of ~1,000 bubbles[21].

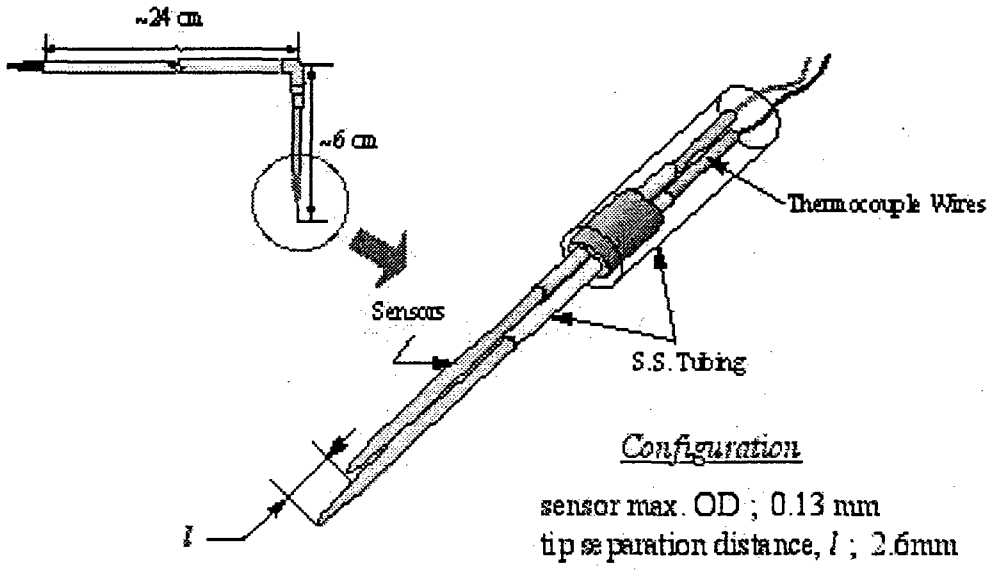

Figure 3. Schematic diagram of the double-sensor conductivity probe and its geometric configuration.

In fabricating the double-sensor conductivity probe, gold acupuncture needles with max. O.D of 0.13mm are employed as the sensors of the probe. The high electrical conductivity of the gold, and its sharply tapered tip make the acupuncture needle ideal as a sensor of the conductivity probe. The sensors of the probe are coated with a low viscous (200 cps at 25°C) and highly adhesive conformal dielectric coating material, which forms a very thin (thickness ~ 0.01 mm/treatment) and uniform coat around the sensors. The coating resin also has a high resistivity ($4x10^4$ ohm/cm), and a strong chemical-proof characteristics, which are essential for the experimental condition. A gauge11 (0.32cm OD) stainless steel tube is used for the probe casing to hold the sensor unit. The 90 degree bend in the casing was constructed with a very small radius so that the probe could be traversed within 3mm of the wall. The simplified schematic diagram and the geometric configurations of the double-sensor conductivity probe used in the present study is shown in Figure 3. The separation distance between two tips of the sensor (l in Figure 3) is chosen as 2.61mm which is approximately 70 % of the mean bubble diameter at given flow conditions as suggested by Wu and Ishii[21]. The detailed fabrication procedures and design of the probe can be found in the study by Kim et al.[23].

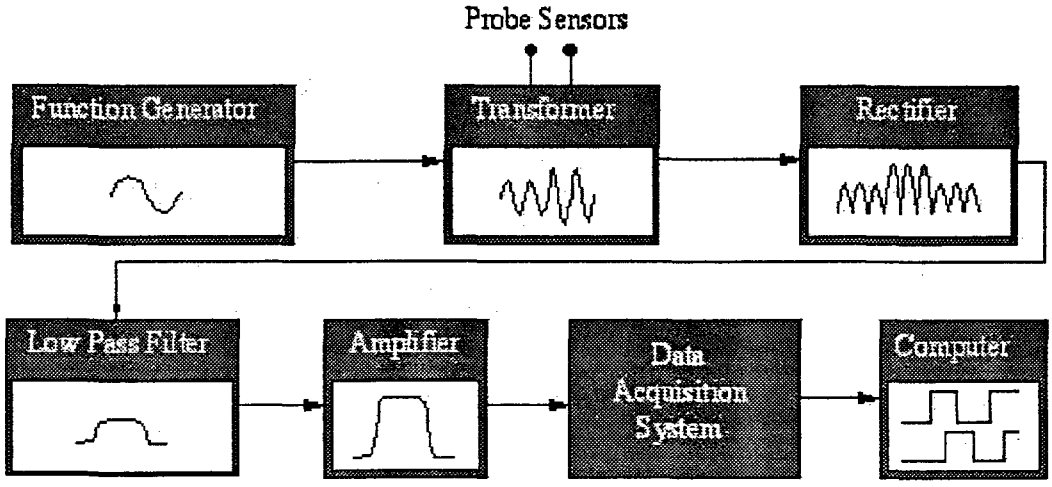

Figure 4. Structure of the AC circuit employed in the double-sensor probe measurement technique.

In order to acquire the signals from the probe, an AC circuit is designed as shown in Figure 4. The AC circuit is chosen in order to minimize the possible oxidation at the tips of the sensors. For the data acquisition system, a DAS1801st board from Keithley, Metrabyte is employed. The sampling frequency is varied between 6 to 8 kHz depending on the flow conditions, and an average of 30sec. of sampling time is acquired in each measurement, which allows thousands of bubbles for one set of data.

3. BENCHMARK OF THE DOUBLE-SENSOR CONDUCTIVITY PROBE TECHNIQUE

The benchmark of the double-sensor probe is performed by employing the image analysis method[24], because the rectangular flow duct is ideal in view of minimizing image distortion. In capturing images, a rectangular window of 10x6 cm is prepared as shown in Figure 5. The location of this window is chosen at the same location where the double-sensor conductivity probe is located. The images of the bubbles are captured by a SONY CCD VX-3, Hi-8 video camera at a frame rate of 30 frames/sec. The void fraction of the two-phase mixture is controlled, so that it is below 5% in order to prevent the bubble images from overlapping. A computer code

developed by Zhang and Ishii[25] is used to process the captured images to obtain the location and the diameter of each bubble in a given frame. An example of the photographic images used in image analysis and the coordinate system employed in the image analysis are shown in Figure 5. Here the image is captured at the flow condition of j_g=0.023m/s and j_f=0.315m/s. The y-z plane, or (flow duct depth)x(window height), area-averaged interfacial area concentration at any x position is then calculated by

$$\langle a_i(x)\rangle_{yz} = \frac{\pi \sum_j \left(D_b(x)\right)_j}{A_{yz}} \tag{23}$$

where $D_b(x)$ is the bubble diameter at location x, and A_{yz} is the product of image height and flow duct depth. In order for the data obtained by the double-sensor conductivity probe to be compared effectively, the local time averaged interfacial area concentration acquired along the x-direction should be line-averaged along the y-direction. Therefore, in obtaining the experimental values, the probe is traversed in half-length of the flow duct gap from the center to the wall by a fraction of 1mm assuming that the flow is symmetric along the y-direction. The equivalent values of the interfacial area concentration measured by the probe to the values from image analysis method is then given by

$$\langle a_i(x)\rangle_{y,probe} = \frac{1}{L_y}\int_0^{L_y} \bar{a}_i^t \, dy \quad , \tag{24}$$

where L_y is the total length of the flow duct gap width.

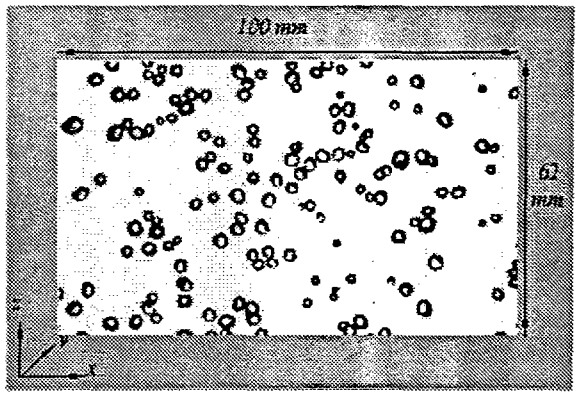

Figure 5. Photographic image captured for image analysis in benchmarking the double-sensor conductivity probe and its coordinate system. j_g=0.023m/s and j_f=0.315m/s

The typical result from a number of experiments is shown in Figure 6. The relative percent difference between the two-methods is within ± 10%. Therefore, considering the limitation of the image method near the edge of the viewing window (as shown in Figure 5), the agreement is acceptable, which benchmarks the double-sensor probe technique.

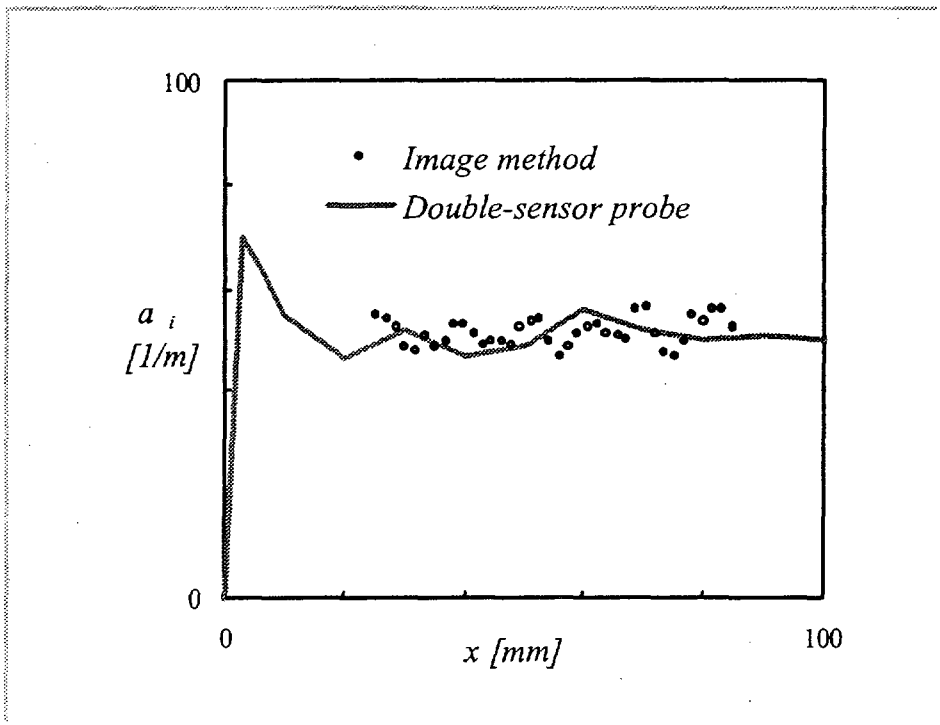

Figure 6. Typical results obtained from the comparison between the interfacial area concentration measured by the double-sensor probe and that from image analysis.

4. EXPERIMENTAL FACILITIES

The present experimental loop includes the injection unit, test section, upper plenum, and the liquid and gas delivery systems. The flow duct is made of transparent acrylic Lucite for flow visualization with flow cross-sectional area of 1x20 cm. Use of this geometry permits unambiguous visualization of the two-phase flow patterns without the distortion caused by curved

surfaces. The loop is operated under atmospheric pressure, and the water and air are supplied by a centrifugal pump and an air-compressor, respectively. The test section is extended up to L/D_h=96.5, along which four measurement ports are installed at L/D_h=6.7, 33.3, 60.0, and 86.7, respectively. After the test section, the flow is introduced into the upper plenum after which the two-phase mixture and the mists are guided into the separator and re-circulated through the test section.

Due to the limiting size of the gap of the flow duct, a side delivery bubble injection unit is designed as shown in Figure 7. To achieve a near-uniform injection of a two-phase mixture, six injection sites, three on each side of the duct width, are drilled. Air bubbles are sheared from the pores of cylindrical porous sparger units by the liquid and introduced into the test section. The six injection sites are designed in such a way that they are offset in equal spacing relative to each other to minimize bubble interactions at the inlet. The incident angles of these sites with respect to the test section are chosen as 13° to avoid disturbance to the injecting bubbles due to sudden expansion of the flow area. The inlet edges are tapered for smooth injection of the two-phase mixture.

The total liquid flow rate(j_{fTot}) is achieved by two liquid inlet sections; one through the two-phase mixture side injection unit(j_{f1}) with which bubbles are sheared from the porous tubes, and another through the three auxiliary lines (j_{f2}) located on the side near the bottom of the flow channel. A honeycomb straightening unit is installed between the auxiliary liquid injection sites and the two-phase mixture injection sites to achieve a uniform liquid flow at the inlet. A stable supply of air (j_g) is established by installing a pressure regulator before the air inlet to the flow meter. Prior to both air and water injection lines, cylindrical mixing chambers are installed so that the inlet condition at each injection site is uniform. For the experiment presented at this time, j_{f1} is fixed at 0.126 m/s while j_{f2} is varied accordingly to achieve desired total liquid injection rates.

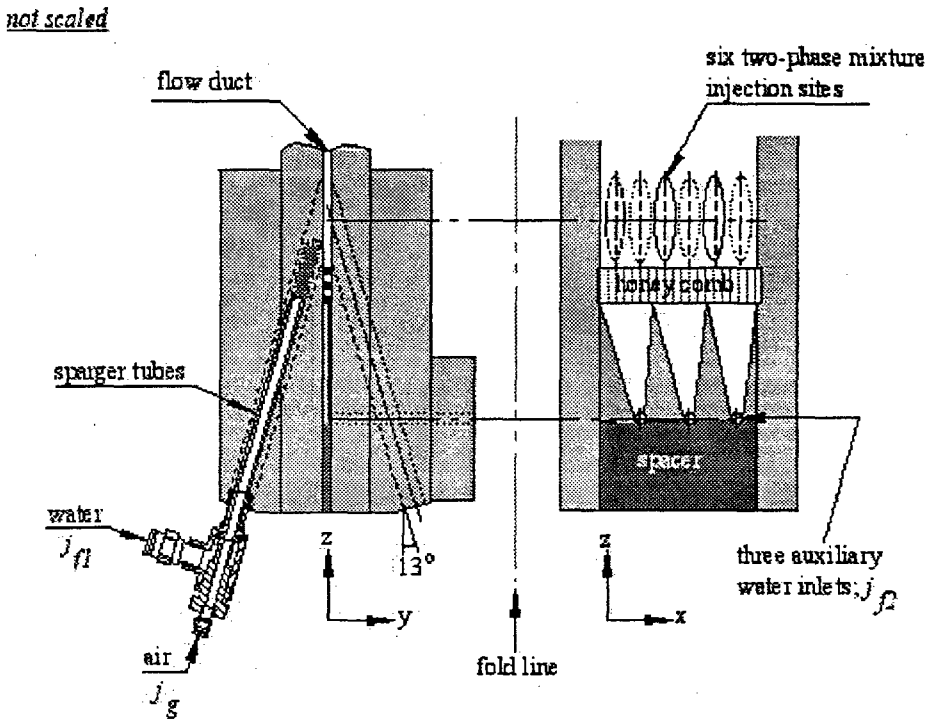

Figure 7. The schematic diagram of the cross-sectional view of the two-phase mixture injection unit, viewed in two (x and y) directions.

5. EXPERIMENTAL RESULTS AND DISCUSSIONS

In the present paper, experimental results from 5 different flow conditions are presented. All of the 5 flow conditions are within the bubbly flow regime as shown in Figure 8(a). The superficial gas velocity is varied between 0.05 and 0.19 m/s, while the total superficial liquid velocity is varied between 0.32 and 1.89m/s. The measurement are made in both lateral (or x and y, respectively) and axial (or z) directions, where the duct-width is denoted as x-direction and the duct-gap as y-direction. Four probe ports are installed along the axial direction of the test section. The probe ports 1 through 4 are located at L/D_h=6.7, 33.3, 60.0, and 86.7, respectively. The traverse system in the probe port is designed in such a way that the probe can be traversed in both x and y directions at a fraction of 1mm. The cross-sectional measurement meshes are established as shown in

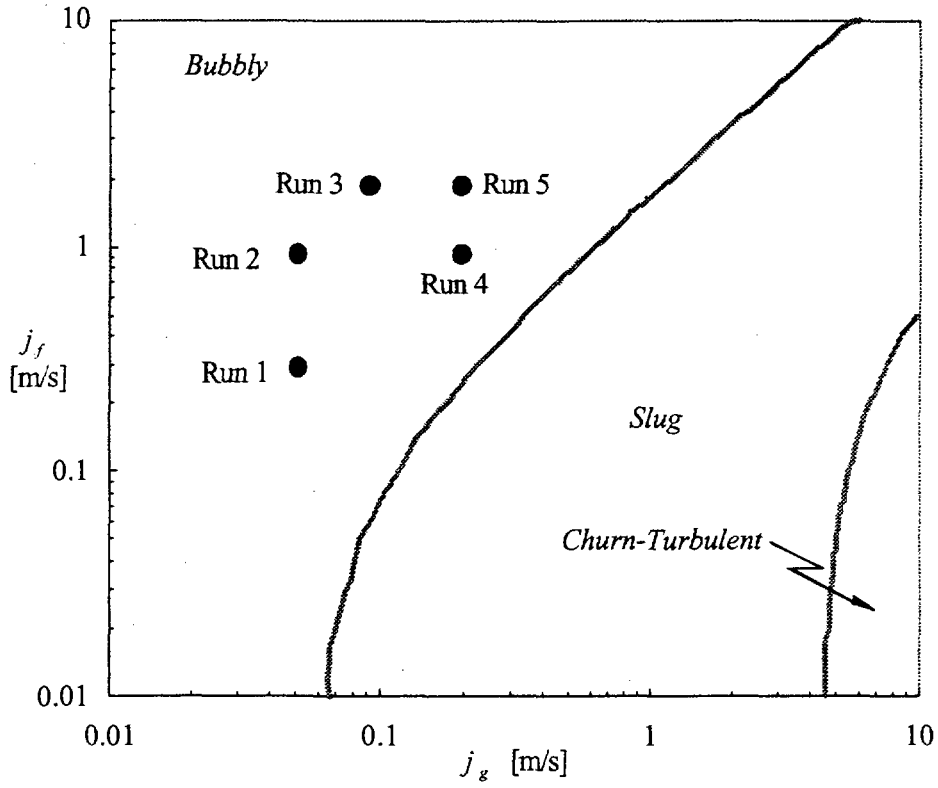

(a) Experimental conditions

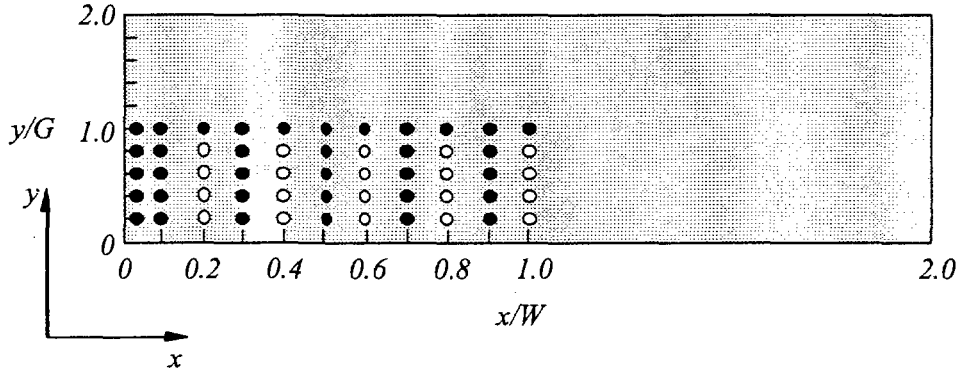

(b) Measurement Matrix

Figure 8. (a) Experimental flow conditions; Flow regime map by Mishima and Ishii[26].
(b) Local measurement locations

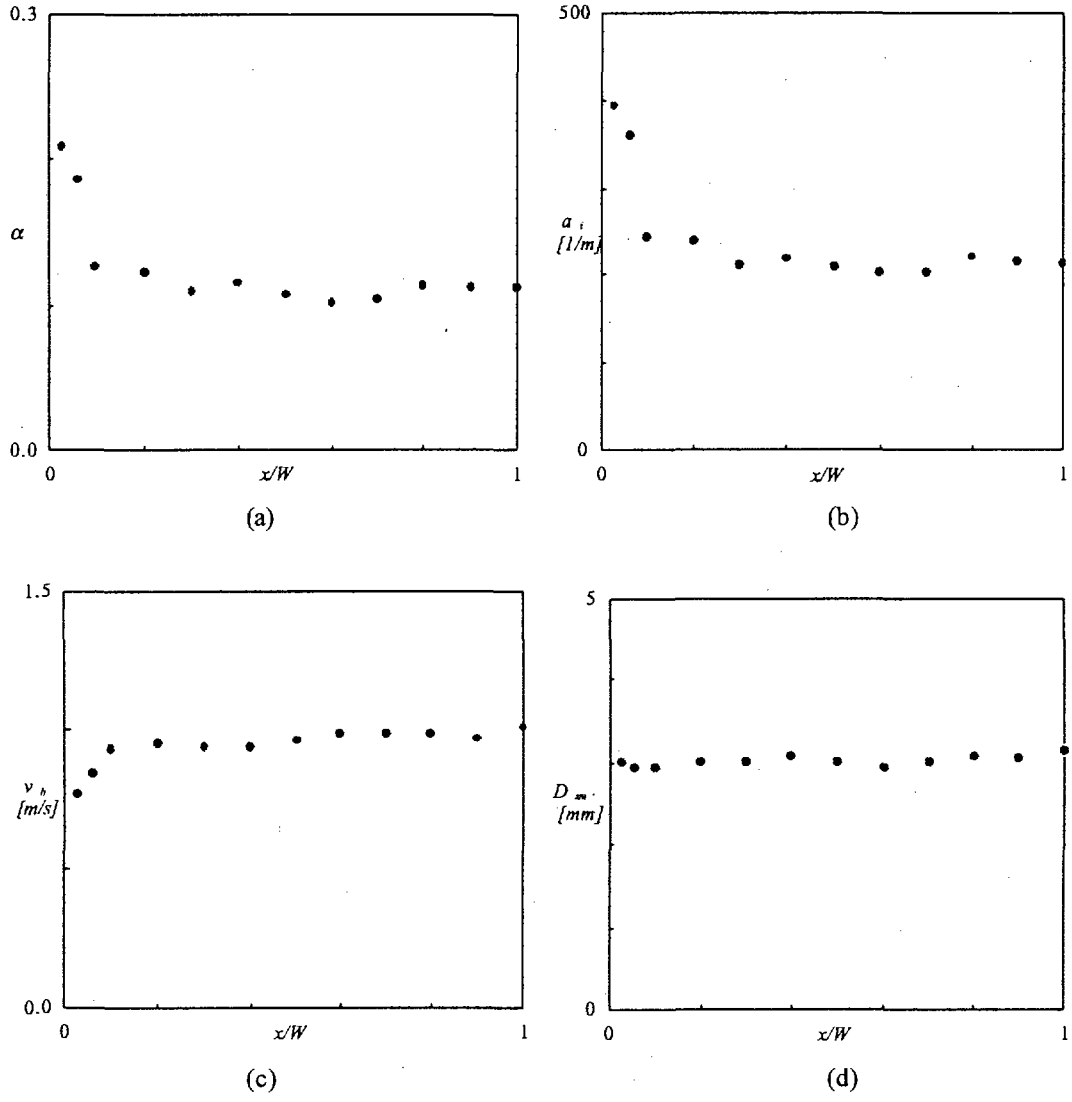

Figure 9. Characteristic experimental results acquired by the double-sensor conductivity probe along the flow duct width for j_g=0.19m/s and j_f=0.95m/s at L/D_h=60. Profiles of y line-averaged (a) void fraction, (b) interfacial area concentration, (c) bubble velocity, and (d) bubble Sauter mean diameter.

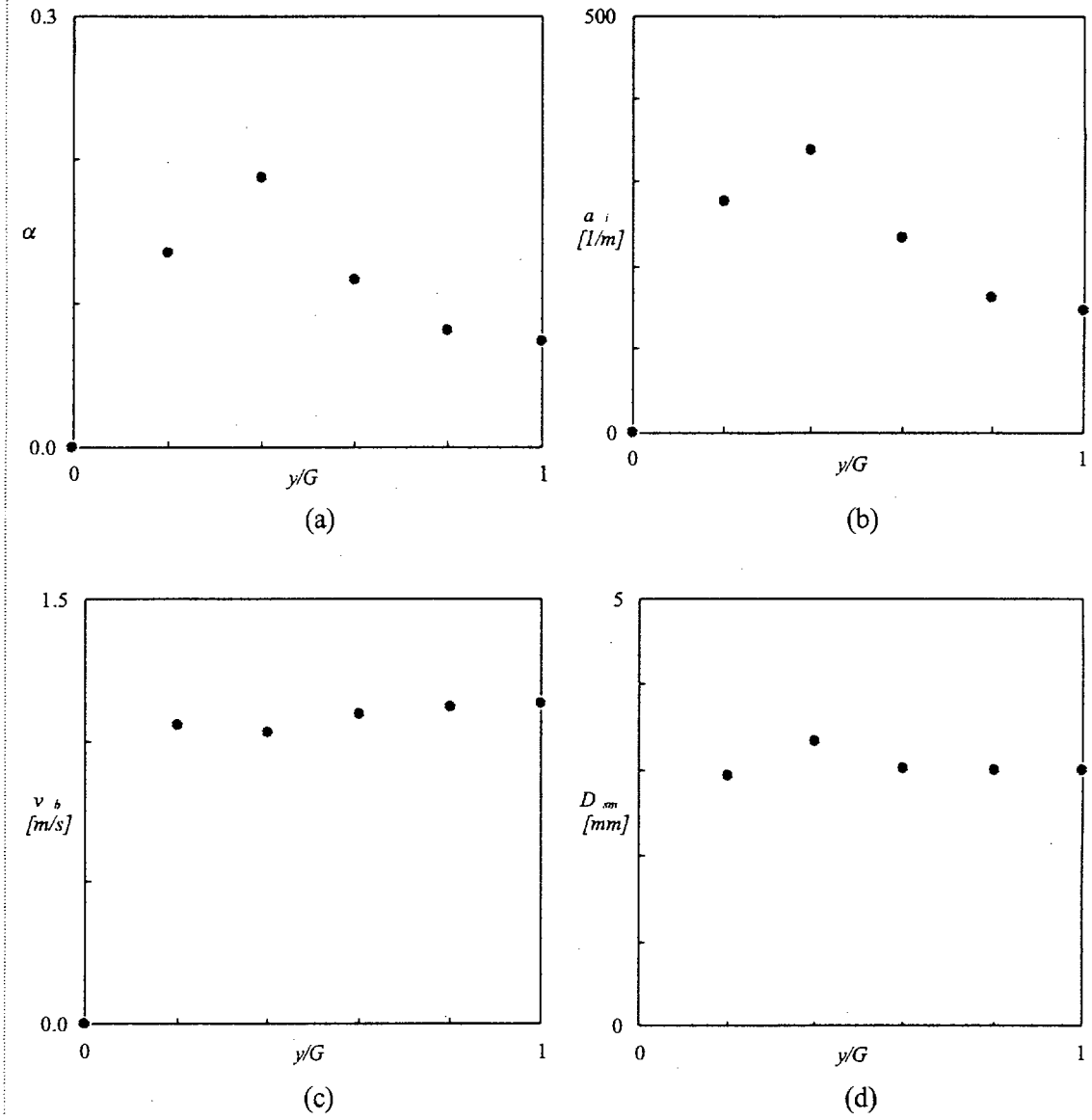

Figure 10. Characteristic experimental results acquired by the double-sensor conductivity probe along the flow gap width for j_g=0.19m/s and j_f=0.95m/s at L/D_h=60. Profiles of local (a) void fraction, (b) interfacial area concentration, (c) bubble velocity, and (d) bubble Sauter mean diameter at x/W=0.9.

Figure 8(b), based on two important factors, namely; the degree of variation of two-phase parameters across the cross-sectional flow area and the extrapolation method employed for the purpose of data processing. In extrapolating the data between the two measurement points, the second-order, two-dimensional Taylor expansion is employed. In Figure 8(b), the measured data points are denoted as solid circles, whereas the extrapolated data points are shown as blank circles. This extrapolation process was necessary in order to obtain the area-averaged parameters across the flow area at each axial measurement location.

The characteristic results of the experimental data are shown in Figure 9(a) through 9(d). Shown here are the data along the width (or x) averaged over the duct gap (y) from Run 4 at L/D_h=60. In the figures, the data are plotted along the non-dimensionalized duct width x/W, with W denoting the half of the duct width. Characteristic peak near the duct wall was apparent in both the void fraction and interfacial area concentration profiles as shown in Figure 9(a) and (b). The wall peak phenomenon is observed in 2 out of 5 flow conditions examined, namely Run 2 and Run 4. In flow conditions such as Run3 and Run5, this phenomenon is weaker and the local peak moves more toward the center of the duct width or duct gap. In Run3 and Run5, two peaks tend to form by peaking near the center, even though not significant. In Figure 9(c), the profile of the bubble velocity v_b, is presented. It is similar to that of liquid turbulent velocity profile and is quite uniform along the width except very near the wall (or x/W 0.1). Furthermore, the bubble Sauter mean diameter is plotted in Figure 9(d). Here the Bubble Sauter mean diameter is calculated by

$$D_{sm} = \frac{6\alpha}{a_i}, \tag{25}$$

It is approximately 3mm and uniform across the duct width. Similar trends are observed in the local profiles of two-phase parameters along the flow duct gap. In Figure 10, the local two-phase flow parameters obtained at x/W=0.9 are plotted along the duct gap (or y) for the same condition as in Figure 9. Here, the data is plotted with respect to the non-dimensional length, y/G, where G denotes the length of half the duct gap. As in the previous case, characteristic wall peak is observed in both void fraction and interfacial area profiles, and the bubble velocity and the bubble Sauter mean diameter remain nearly uniform across the duct gap.

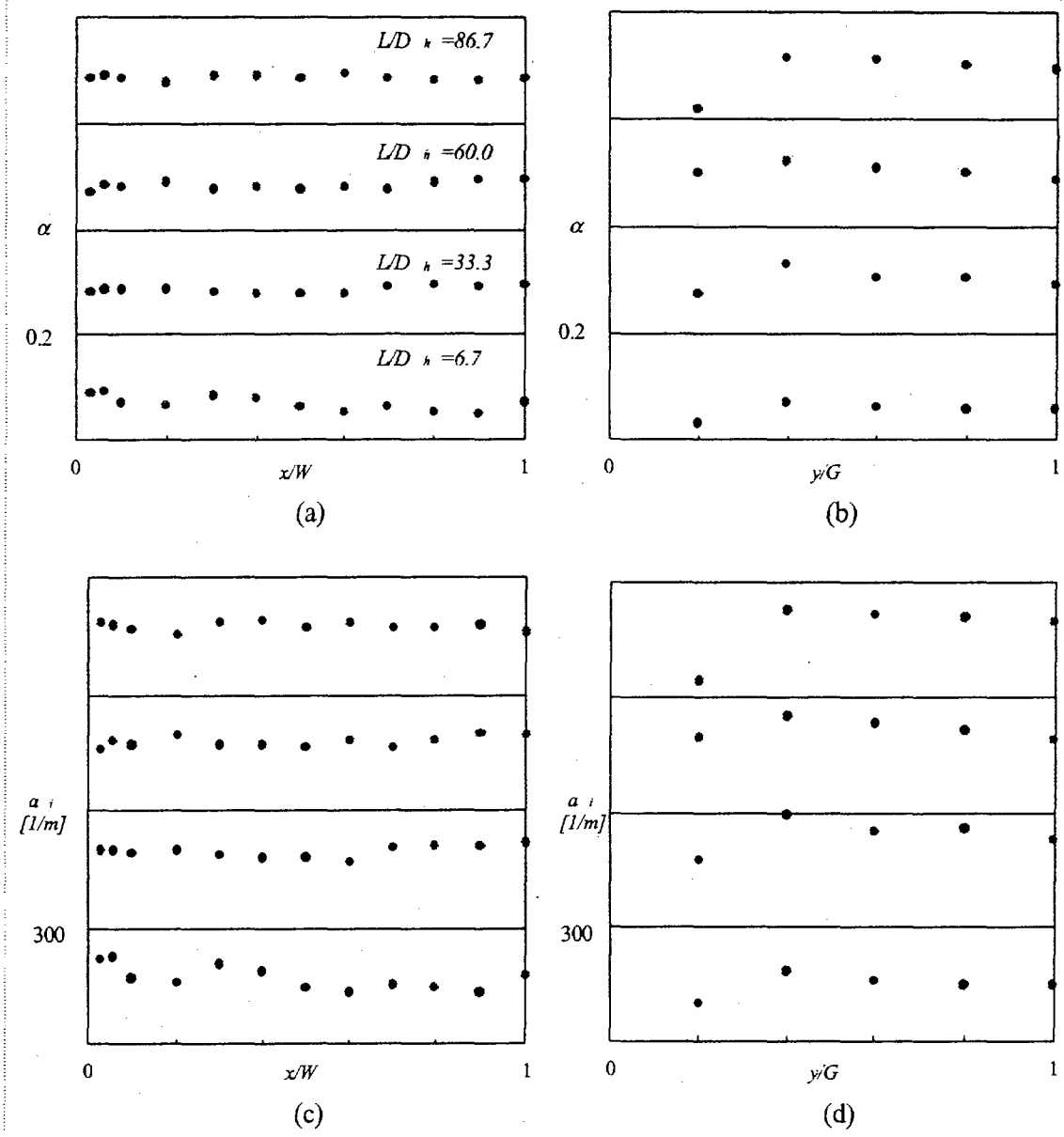

Figure 11. Profiles of local void fraction and interfacial area concentration for Run 1 along the duct-width and the duct-gap at four axial measurement locations. Flow conditions for Run 1; j_g=0.05 and j_f=0.32m/s.

In Figure 11, the data from Run 1 are plotted with respect to the flow duct width and the gap at each of the four axial measurement locations. As mentioned earlier, in this flow condition both void fraction and interfacial area concentration profiles remain quite uniform across both the flow duct width and the gap.

To provide for examination of the interfacial area transport and bubble interactions, the local interfacial area concentration is area-averaged across the flow area and plotted along the axial flow direction in Figure 12(a). As can be seen in this figure, the change in the area- averaged interfacial area concentration along the flow direction is small. However, considering the pressure change and bubble expansion along the flow duct, the decreasing or nearly-uniform trend of the $<a_i>$ implies active coalescence mechanisms in the flow conditions examined. Also in Figure 12(b), the area-averaged interfacial area concentration is plotted with respect to the area-averaged void fraction regardless of the flow conditions or measurement location. As shown in this figure, a linear relationship can be observed between the two parameters, which implies that the bubble sizes remain uniform and verifies equation (25). In the present study, the average bubble Sauter mean diameter is approximately 3mm.

Finally, the experimental data are plotted with respect to the estimation by the drift flux model given by

$$< j_g > \Big/ < \alpha > = C_0 < j > + << V_{gj} >> \tag{26}$$

In the present analysis, the distribution parameter C_o is chosen as 1.35 as suggested by Ishii[27] for rectangular duct flows. In estimating $<<V_{gj}>>$, the equation given by Ishii[27] is employed such that

$$<< V_{gj} >> = \sqrt{2}\left(\frac{\sigma g \Delta\rho}{\rho_f^2}\right)^{1/4} \left(1 - \langle\alpha\rangle\right)^{1.75}, \tag{27}$$

which yields an average value of 0.23 m/s. The result is shown in Figure 13. In plotting the data points, the data obtained at L/D=6.7 are omitted accounting for the inlet effect. As can be seen in this figure, the data matches reasonably well with estimation made by the drift flux model.

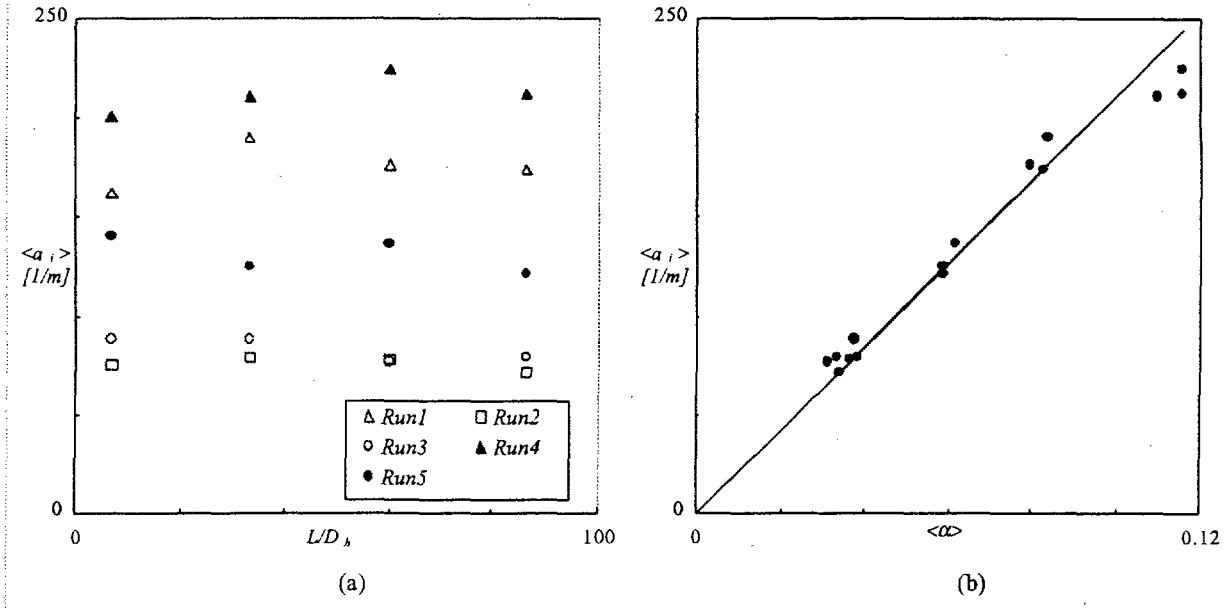

Figure 12. (a) The development of the area-averaged interfacial area concentration along the axial flow direction. (b) The relationship between the area-averaged interfacial area concentration and the void fraction

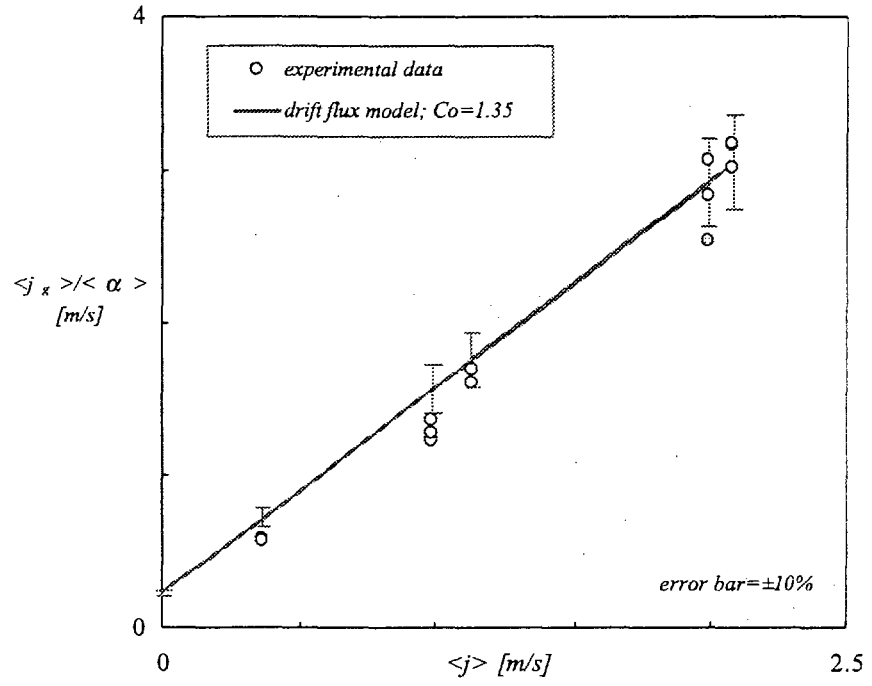

Figure 13. The experimental data and the drift flux model with C_o=1.35 and $<<V_{gj}>>$=0.23m/s.

SUMMARY

An experimental study was performed to examine the detailed structures of confined two-phase flow and to establish the database for the development of an interfacial area transport equation. The measured local two-phase parameters include void fraction, interfacial area concentration, and bubble velocity. The measurements are made by the double-sensor conductivity probe with improved design and improved measurement principles. The measurement error associated with the current double-sensor probe technique is approximately ±7%. The current probe technique is benchmarked by the image analysis method. The difference between the two measurement methods lies within ±10%. The detailed local measurements are made across one quarter of the cross-sectional area of the flow duct at four different axial locations at five different flow conditions within bubbly flow regime.

The characteristic wall peak phenomenon in the profiles of the void fraction and interfacial area is observed in 2 out of 5 flow conditions examined, namely Run2 and Run4. The profiles of the bubble velocity, however, remain fairly uniform being similar to that of the turbulent velocity profile. The uniform bubble velocity profiles are observed along both the duct-width and duct-gap at all flow conditions except at L/D_h=6.7. At L/D_h=6.7, the velocity profiles exhibit a transverse variation due to the inlet condition. Furthermore, the bubble Sauter mean diameter is acquired by using the relation given by equation (25). In all of the flow conditions examined, the bubble Sauter mean diameter remains nearly uniform at approximately 3mm.

The local parameters are area-averaged across the cross-sectional area of the flow duct in order to examine the transport phenomena and interaction between bubbles. The development of the area-averaged interfacial area concentration along the test duct varies depending on the flow conditions. Considering the expansion of the bubbles along the flow duct due to the pressure change, the decreasing or nearly-uniform trend of the $<a_i>$ implies active coalescence mechanisms in the flow conditions examined. This implies that different bubble interaction mechanisms can be dominant depending on the flow conditions.

ACKNOWLEDGEMENTS

This study was performed at Purdue University under the auspices of the Bettis Atomic Power Laboratory, Bechtel Bettis, Inc..

REFERENCE

1. M. Ishii, *Thermo-Fluid Dynamic Theory of Two-Phase Flow*, Collection de la Direction des Etudes et Recherches d'Electricite de France, Eyrolles, Paris, 1975
2. M. Ishii and K. Mishima, Two-fluid model and hydrodynamic constitutive relations, *Nuclear Eng. Design*, **82**, pp. 107-126, 1984
3. T. C. Chawla and M. Ishii, Two-fluid model of two-phase flow in a pin bundle of a nuclear reactor, *Int. J. Heat and Mass Transfer*. **23**, p.991, 1980
4. M. Ishii and N. Zuber, Drag coefficient and relative velocity in bubbly, droplet or particulate flows, *AIChE J.*, **25**, p843, 1979
5. N. Zuber, On the dispersed two-phase flow on the laminar flow regime, *Chem. Eng. Sci.* **19**, p 897, 1964
6. G. Kocamustafaogullari and M. Ishii, Foundation of the Interfacial Area Transport Equation and its Closure Relations, *Int. J. Heat and Mass Transfer*, **38**, No. 3, p481,1995
7. J. N. Reyes, Statistically Derived Conservation Equations for Fluid Particle Flows, *ANS-TANSAO*, **60**, p 669, 1989 ANS Winter Meeting, San Francisco, CA, Nov., 1989
8. Q. Wu, S. Kim, M. Ishii, and S. G. Beus, One-group interfacial area transport in vertical bubbly flow, *Int. J. Heat Mass Transfer*, **41**, Nos. 8-9, pp. 1103-1112, 1998
9. M. Sadatomi, Y. Sato, and S. Saruwatari, Two-phase flow in vertical non-circular channels, *Int. J. Multiphase Flow*, **8**, No. 6, pp. 641-655, 1982
10. H. Ide and H. Matsumura, Frictional pressure drops of two-phase gas-liquid flow in rectangular channels, *Experimental Thermal and Fluid Science*, **3**, 362-372, 1990
11. K. Mishima, T. Hibiki, and H. Nishihara, Some Characteristics of Gas-Liquid Flow in Narrow Rectangular Ducts, *Int. J. Multiphase Flow*, **19**, No. 1, pp. 115-124, 1993
12. T. Wilmarth and M. Ishii, Two-phase flow regimes in narrow rectangular vertical and horizontal channels, *Int. J. Heat Mass Transfer*, **37**, No. 12, pp. 1749-1758, 1994
13. L. G. Neal and S. G. Bankoff, A high resolution resistivity probe for determination of local void properties in gas-liquid flow, *AIChE J.*, **9**, pp. 490-494, 1963

14. I. Kataoka., M. Ishii, and A. Serizawa, Local formulation and measurements of interfacial area concentration in two-phase flow, *Int. J. Multiphase Flow*, **12**, No. 4, pp. 505-529, 1986

15. I. Kataoka and A. Serizawa, Interfacial area concentration in bubbly flow, *Nuclear Eng. Design*, **120**, pp. 163-180, 1990

16. M. Ishii and S. T. Revankar, Measurement of interfacial area using four-sensor probe in two-phase flow, *Purdue University Report*, PU NE-91-1, 1991

17. S. T. Revankar and M. Ishii, Local interfacial area measurement in bubbly flow, *Int. J. Heat Mass Transfer*, **35**, No. 4, pp. 913-925, 1992

18. I. Kataoka, M. Ishii, and A. Serizawa, Sensitivity analysis of bubble size and probe geometry on the measurements of interfacial area concentration in gas-liquid two-phase flow, *Nuclear Eng. Design*, **146**, pp. 53-70, 1994

19. G. Kocamustafaogullari, W. D. Huang, J. Razi, Measurement and modeling of average void fraction, bubble size and interfacial area, *Nuclear Eng. Design*, **148**, pp. 437-453, 1994

20. W. H. Leung, S. T. Revankar, Y. Ishii, and M. Ishii, Axial development of interfacial area and void concentration profiles measured by double-sensor probe method, *Int. J. Multiphase Flow*, **38**, No. 3, pp. 445-453, 1995

21. Wu, Q. and Ishii, M., 1999, Sensitivity study on double-sensor conductivity probe for the measurement of interfacial area concentration in bubbly flow, *Int. J. Multiphase Flow*, **25**, No. 1, pp. 155-173, 1999

22. S. Kim, X. Y. Fu, X. Wang, and M. Ishii, The local interfacial area concentration measurement in a two-phase flow using a four-sensor conductivity probe, *ANS-TANSAO* **79**, p. 356, 1998 ANS Winter Meeting, Washington DC, Nov. 15-19, 1998

23. S. Kim, Q. Wu, and M. Ishii, Fabrication Procedure and Design of a double-sensor conductivity probe, *Purdue University Report*, PU NE-97-1, 1997

24. Q. Wu, S. Kim, D. McCreary, M. Ishii, and S. G. Beus, Measurement of interfacial area concentration in two-phase bubbly flow, *ANS-TANSAO* **77**, p. 437, 1997 ANS Winter Meeting, Albuquerque, NM, Nov. 10-20, 1997

25. G. Zhang and M. Ishii, Isokinetic sampling probe and image processing system for droplet size measurement in two-phase flow, *Int. J. Heat and Mass Transfer*, **38**, p 2019, 1995

26. K. Mishima and M. Ishii, Flow regime transition criteria for upward two-phase flow in vertical tubes, *Int. J. Heat Mass Transfer*, **27**, No. 5, pp. 723-737, 1984

27. M. Ishii, One-dimensional drift-flux model and constitutive equations for relative motion between phases in various two-phase flow regimes, *Argonne National Laboratory Report*, ANL-77-47, 1977